Draft version September 1, 2021
Typeset using LaTeX **twocolumn** style in AASTeX631

Tracing OH absorption to illuminate H_2 along the line of sight to Cassiopeia A

Rebekah Polen[1,2] and Pedro Salas[1]

[1] *Greenbank Observatory*
Greenbank, West Virginia, USA
[2] *Randolph-Macon College*
Ashland, Virginia, USA

ABSTRACT

The dense interstellar medium is defined by regions of molecular hydrogen, or H_2. Observations of these regions have presented challenges due to the nature of the dihydrogen molecule and its relative invisibility to the observer. Therefore, gas tracers are used to map the dense medium in molecular hydrogen's place. Carbon monoxide, or CO, is the second most abundant molecule in the interstellar medium and the most common tracer for H_2. The problem with CO as a molecular hydrogen tracer is that it most likely does not trace H_2 exactly and leaves uncertain CO-dark regions, or places where CO is not present where H_2 still is. The inability to map molecular hydrogen directly leaves science to assume these regions exist with unclear boundaries. Observing less common gas tracers, such as the hydroxyl radical OH, a better image of the dense interstellar medium and therefore molecular hydrogen can be pieced together. By comparing column densities that have been converted to molecular hydrogen, gas tracers can be directly and visually compared to one another in how well they probe H_2. OH observations on the Expanded Very Large Array (EVLA) suggest a complimentary relationship to CO in mapping H_2, which holds significance in further study of the dense interstellar medium and star formation.

Keywords: The interstellar medium — Radio astronomy — Cassiopeia A — Molecular gas

1. INTRODUCTION

The dense, molecular regions of the interstellar medium (ISM) are defined by the presence of molecular hydrogen, or H_2, because for hydrogen to be able to bond with itself there must be a higher density of atoms present. However, H_2 cannot be seen except under special conditions, such as along the line of sight to nearby stars in the ultraviolet. It is the lack of a permanent dipole moment that causes this issue. Carbon monoxide (CO) happens to be an excellent placeholder for H_2, as it is the next most abundant molecule. Therefore, by observing CO in the ISM we can roughly trace regions of dense molecular hydrogen. The only problem with this method of using a gas tracer is that it cannot be known how well CO traces the unseen H_2. CO may or may not trace H_2 exactly. One way of bridging this gap is to observe other, less common gas tracers of the dense ISM to see how they compare to CO in tracing H_2 so that CO-dark regions, or regions where CO is invisible or poorly traces, may be illuminated. This research focuses on the hydroxyl radical (OH) as a candidate for observing CO-dark molecular gas.

Attempting to study the dense ISM more accurately holds importance in various fields of astrophysics, most notably star formation. Dense clouds in the interstellar medium are host to star forming regions, although there are no notable star forming regions in the immediate area around the target of observation, Cassiopeia A.

Cassiopeia A is a supernova remnant (SNR) that exploded in the late 17^{th} century in a Type IIb core collapse supernova Zhou et al. (2018). Located on the edge of the Perseus arm of the Milky Way Galaxy, the SNR is about 11,000 light years, or 3.4 kpc, from Earth Oonk et al. (2017). Cassiopeia A is one of the brightest radio sources in the sky outside our Sun, and its history is somewhat unclear with regards to its exact age and progenitor star, although Weil et al. (2020) suggest that it came from a red supergiant.

Astronomers have been looking to Cassiopeia A in the radio regularly to study the interstellar medium due to its excellent position in our galaxy that enlightens the gases positioned between the remnant and Earth. Kirchhoff's second law illustrates why this is important, as a hot opaque surface viewed through a relatively

cool transparent gas will provide an absorption spectra. These spectra, seen as dark lines of absorption within a continuum spectrum, can be studied and hold information regarding that gas. The position of the remnant is unique here because it is far enough behind the gas of the Perseus arm to illuminate it, but not interact with it. Carbon radio recombination line (CRRL) research puts the main component of the gas of -47 km s^{-1} at 100 pc in front of the remnant Salas et al. (2018). Additionally, the slightly elevated temperature of the gas in front of the remnant was found to be caused by background cosmic rays in the Milky Way and not by shocks from the SNR Zhou et al. (2018).

Therefore, the interstellar gas being studied is undisturbed by the winds or shocks of the remnant Zhou et al. (2018). For this reason, the young age of Cassiopeia A is key to its importance in studying the ISM as its shell has not expanded out far enough to interact with its local giant molecular cloud (GMC), creating an ideal environment for observation.

2. METHODS

This research used preexisting data from Arias et al. (2018) and from Dr. Ping Zhou[1] at Nanjing University seen in Zhou et al. (2018). In particular, four EVLA OH data cubes on 1612-, 1665-, 1667-, and 1720-MHz from Arias et al. (2018) and the IRAM 1-0 transition cube of CO from Zhou et al. (2018) of the (1-0) 13CO isotopologue. The 13CO isotopologue was specifically chosen for comparison to OH as opposed to 12CO due to its optical thinness. OH is optically thin, and comparing it to 13CO is therefore more accurate than optically thick 12CO. Additionally, an archival data cube of a continuum L-band observation on Cassiopeia A taken on the EVLA in 2017 was used for analysis and can be seen in Figure 1, also seen in Arias et al. (2018).

All cubes were convolved and reprojected to 22" (arcseconds) using a Gaussian kernel within Astropy and its associated packages to maintain the same spatial resolution and dimensions (Robitaille et al. (2013); Price-Whelan et al. (2018)). The resolution of 22" was chosen based on the resolution of the CO cube to which the OH cubes could be equated. Since resolution cannot be increased, all cubes have to be smoothed over to the lowest resolution which was 22". The OH data cubes have a spectral resolution of 976 Hz on a channel width of 2 MHz. Pixel resolution within the images is 3" by 3", and all work was conducted within Jupyter and DS9.

[1] Dr. Ping Zhou, Nanjing University: ORCiD Page. Data kindly provided upon request.

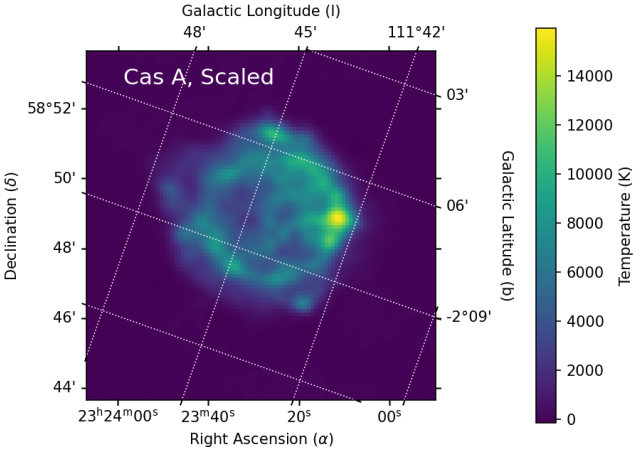

Figure 1. Continuum image of Cassiopeia A in the L-band, Expanded Very Large Array, 2017.

3. RESULTS AND ANALYSIS

In this section the methods of analysis and generating results are discussed chronologically. The OH data was confirmed to be in local thermodynamic equilibrium, passed through a variety of equations to ultimately calculate column density, and finally converted to molecular hydrogen column density so that it could be visually compared to CO.

3.1. *Assumption of LTE*

In order to derive any physical properties from the absorption lines of hydroxyl, it first had to be confirmed that the gas was in local thermodynamic equilibrium (LTE). The equations and methods outlined in the literature over the last few decades use an assumption of LTE to make analytical conclusions about the properties of the gas more easily due to the equalized temperature in the region. Alternative, potentially more accurate methods for measuring properties like excitation temperature require both an emission and absorption spectra, but Cassiopeia A is too bright of a radio source to extract an emission spectrum for OH even when looking off the face of the shell.

Before LTE could be confirmed on the OH data, the -47 km s^{-1} component of the gas had to be confirmed to be genuine signal. First, the absorption lines were analyzed assuming a Gaussian fit to the line profiles based on the nature of thermal random motion in gas particles. By assuming a Gaussian fit to these profiles, 99.7% of noise will fall within 3 σ (3× the standard deviation) of the main region of data. 3 σ lines were overlaid on absorption spectra from both the main lines in Figure 2 to show that the lines lie outside the 3 σ range and

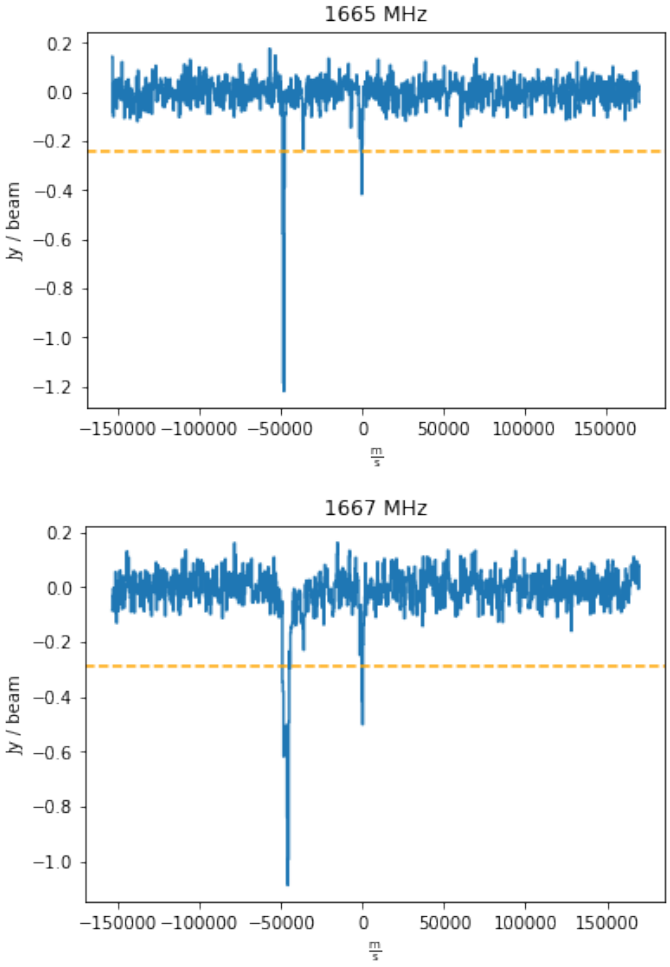

Figure 2. Signal regions for the 1665- and 1667-MHz absorption lines of hydroxyl with overlaid 3 σ boundary lines. Local material sitting at 0 km s^1 crosses the line, but this research addresses the gas sitting at -47 km s^{-1} within the Perseus Arm.

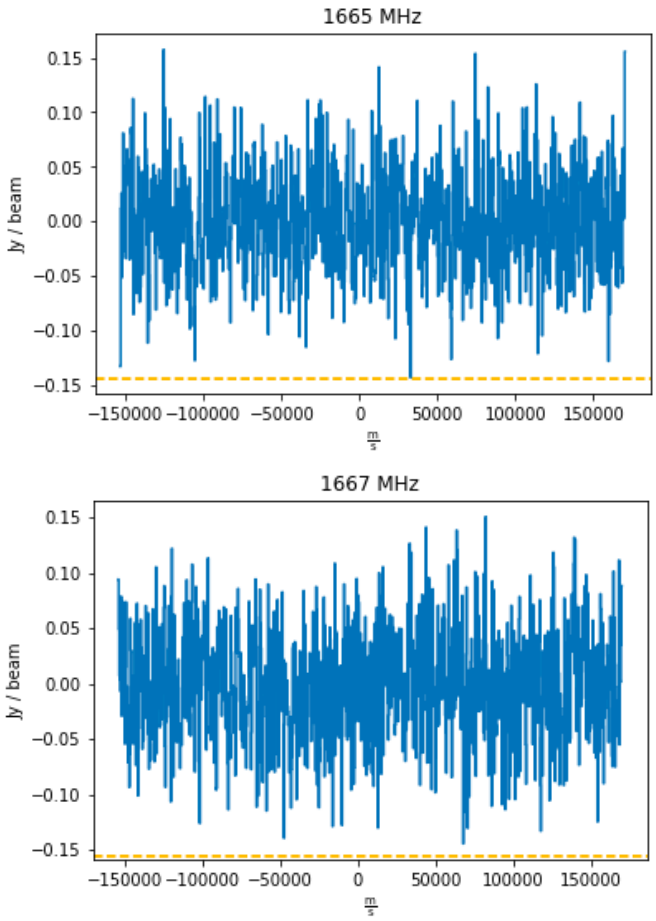

Figure 3. Noise regions for the main lines of 1665- and 1667-MHz. Dashed lines are overlaid at the 3 σ boundaries showing that this data does not represent signal.

can be assumed to be signal. This method did not allow the satellite lines of OH to be considered signal (1612- and 1720-MHz). An example of the noise can be seen in Figure 3, which represents regions of the main lines where absorption is not expected. No portion of the noise crosses the dashed 3 σ line and no dips are visibly distinguishable in the plot.

In order to check for LTE in the main lines of hydroxyl, the lines were compared to each other by the ratios as listed by Ebisawa et al. (2015). Here, the ratio for the lines of OH in LTE are 1:5:9:1 along 1612:1665:1667:1720 MHz lines. Therefore, the 1665 line should be $\frac{5}{9}$ the 1667 line. Figure 4 shows how this ratio is followed very clearly, with -0.5 and -0.9 lines overlaid for reference. Visibly, this shows how the 1665 line is almost exactly $\frac{5}{9}$ the 1667 line. The satellite lines of OH did in fact follow this ratio, but since the signal-to-noise ratio was so low, they were not included regardless. At this point, the scope of research was narrowed to the two main lines of hydroxyl, 13CO, and the continuum data cube. Additionally, based on signal-to-noise, the components of gas in the Perseus Arm of the galaxy aside from -47 km s^{-1} were too weak to analyze. The research scope was narrowed to only the -47 km s^{-1} component.

3.2. *OH Equations*

With the main lines of hydroxyl in local thermodynamic equilibrium, equations from two papers were used to extract information about the optical depth, excitation temperature, and column density of the data. First, equations 1 and 2 were implemented using python in Jupyter Lab to generate plots of optical depth and excitation temperature. These equations required the main lines' data cubes for brightness temperature, which was converted from Jy $beam^{-1}$ into K before it was passed through the equation. The continuum image of Cassiopeia A, rendered in Figure 1, was converted to K and

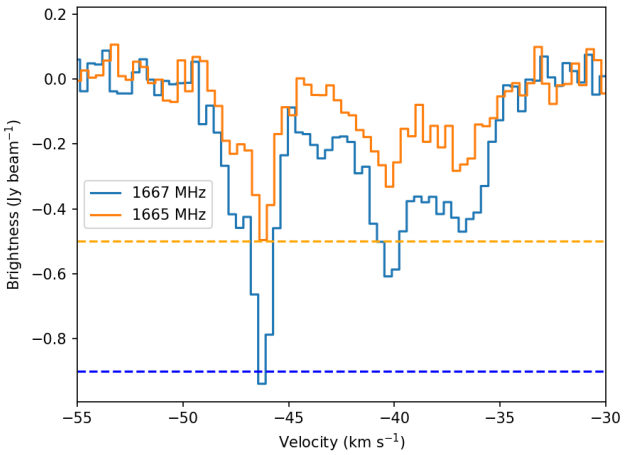

Figure 4. Spectra for the 1665- and 1667-MHz absorption lines of hydroxyl on -50 to -30 km s^{-1}. Orange is the -0.5 line and blue is the -0.9 line for visual reference to the 1:5:9:1 ratio.

used as well for the continuum temperature, T_c, variable in the equations.

$$T_b(1667) = (T_{ex} - T_c)(1 - e^{-\tau_{1667}}) \quad (1)$$

$$T_b(1665) = (T_{ex} - T_c)(1 - e^{-\tau_{1667}/1.8}) \quad (2)$$

Here,[2] $T_b(1665)$ and $T_b(1667)$ are the brightness temperatures of the main lines, T_{ex} is the excitation temperature, T_c is the continuum temperature, and τ is the optical depth. Equations 1 and 2 can be solved with mild algebraic manipulation to isolate both excitation temperature T_{ex} and optical depth τ (Dawson et al. (2014)). In LTE, The optical depth should be the same for both main lines differing only by the 5:9 ratio described in Ebisawa et al. (2015), which is seen by the $\frac{1}{1.8}$ value in equation 2. The optical depths are represented in Figure 5. Excitation temperature is represented in Figure 6, however, it traces the continuum image of the remnant very closely. This result suggests a problem which was warned of within the literature that the excitation temperature and the background temperature are so similar it is not detectable Keohane et al. (1996). Using Keohane et al. (1996) and Zhou et al. (2018), an educated assumption was made of the excitation temperature to be 15 Kelvin. In actuality, the excitation temperature is not a constant but something that would vary over the face of the remnant.

[2] Equations 6 and 7 in Dawson et al. (2014)

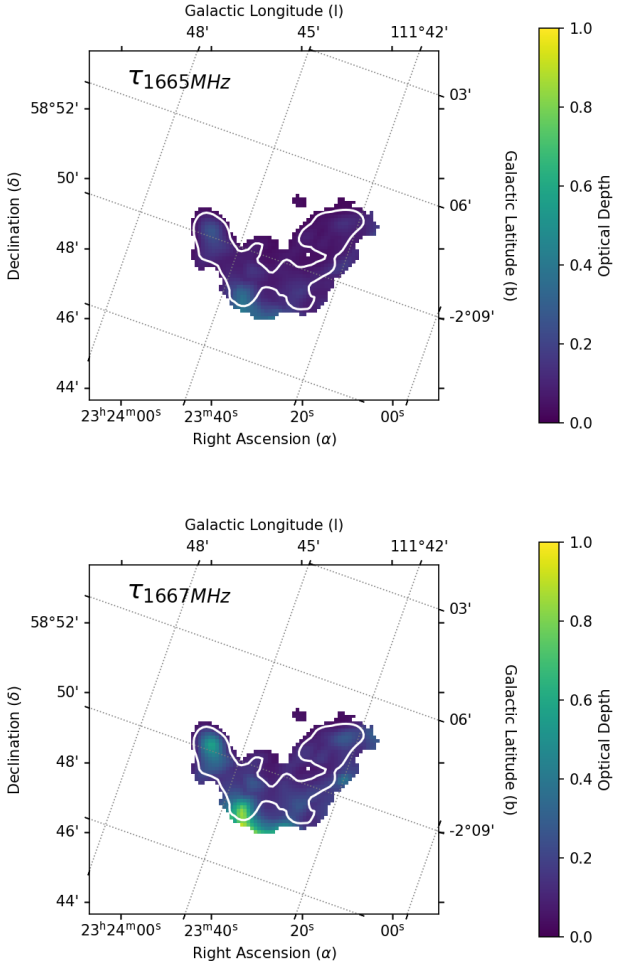

Figure 5. Calculated optical depths for both main lines of hydroxyl at 1665- and 1667-MHz. The optical depth of 1665-MHz is $\frac{5}{9}$ the values of 1667-MHz which is visually noticeable.

$$N(OH) = 2.39 \times 10^{14} T_{ex}(1667)\tau_0(1667)\Delta v \quad (3)$$

Here,[3] N_{OH} is the column density of the OH, and Δv is the velocity dispersion. Equation 3 calculates the column density of the OH using the optical depth and excitation temperature plots as well as a velocity dispersion map, or moment 2 map, which can be seen in Figure 7.

The final step in analyzing OH and CO so that they may be compared to one another was converting both column densities into molecular hydrogen. Essentially, the OH and CO plots of column density can be multiplied by a conversion factor to represent molec-

[3] Equation 8 in Dawson et al. (2014)

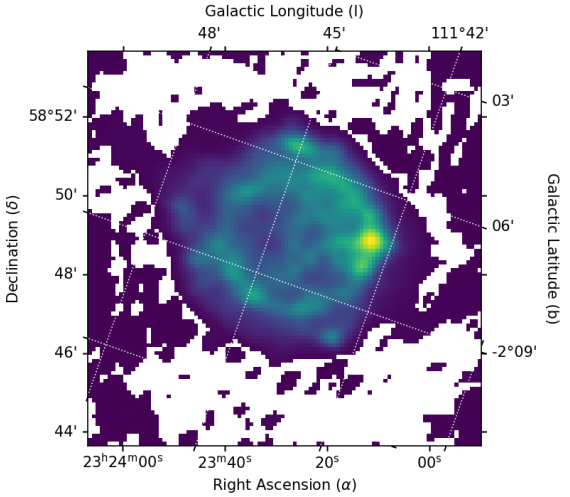

Figure 6. Calculated excitation temperature for OH. The resemblance of this image to Figure 1 suggests that the background temperature and the excitation temperature are indistinguishable.

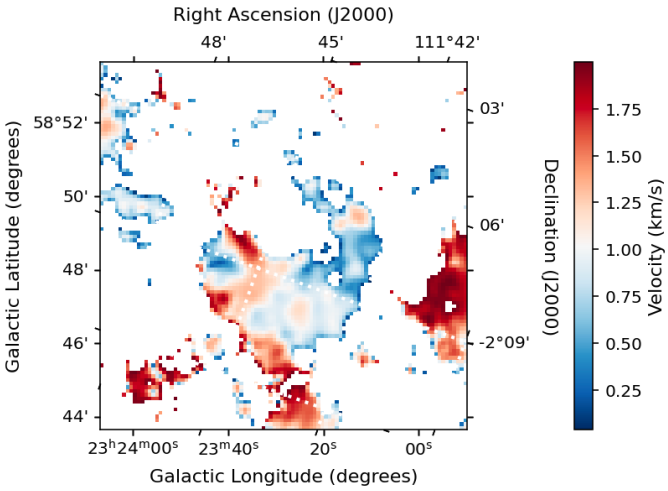

Figure 7. Moment 2, or velocity dispersion, map for OH on the main absorption lines. This image was passed through Equation 3 to calculate column density.

ular hydrogen column density instead. 13CO is more well-documented and has a known conversion factor of 2×10^{-6}. Calculating the conversion factor for OH was done using equation 4 Keohane et al. (1996).

$$\frac{N_{OH}}{N_{H_2}} = (4.1 \pm 2.7) \times 10^{-6} (\frac{T_{ex}}{20K}) \quad (4)$$

Here,[4] N_{H_2} is the column density for molecular hydrogen. The estimated excitation temperature of 15 K was

[4] Equation 14 in Keohane et al. (1996)

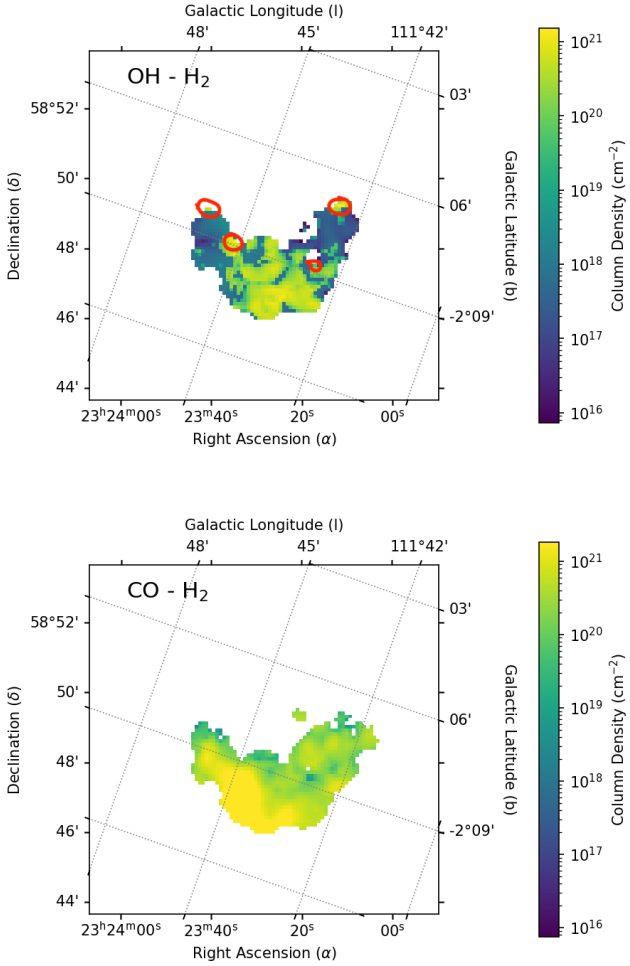

Figure 8. Column density of molecular hydrogen as seen by observing OH and CO respectively. Regions circled in red are spaces where OH illuminates more molecular hydrogen than CO. Both images are on logarithmic scales which were determined in DS9 as best fit.

used here for T_{ex} as well as the plotted column density calculated from equation 3. This equation provided a conversion factor of 5.1×10^{-6}.

3.3. *Results*

The results of this research can be reduced to two plots of column density converted to molecular hydrogen. The molecular hydrogen column density maps calculated with OH and CO are represented in Figure 8

Looking at Figure 8, CO is visibly a more even and abundant tracer of molecular hydrogen than OH. CO is more abundant than OH on an order of over 100 Keohane et al. (1996). Therefore, it is expected that OH will provide a choppier and less abundant plot of column density than CO for molecular hydrogen. However, OH is not bound to CO regions where carbon monoxide is

present. OH, as a molecule in the interstellar medium, is only bound to dense regions of H_2. Carbon monoxide is the second most abundant molecule in the ISM next to H_2, and OH can statistically be present in CO-dark regions. Figure 8 shows how on certain regions the column density of H_2 traced by OH is larger than that traced by 13CO, which confirms that there is H_2 in regions not probed by CO, but rather by less abundant and common tracers.

The results of this research are impacted by the assumptions that were made along the way with excitation temperature as well as local thermodynamic equilibrium. Assumptions can impact the exactness of the results and should be acknowledged.

With regards to Figures 5, 7, and 8 these plots tend to cut out the northern face of the remnant as it is much less rich in gas than the southern face. Therefore, it is often masked as noise.

4. CONCLUSION

Here presented is the analysis and comparison of OH to CO as a tracer of the dense interstellar medium. CO is and continues to be an excellent and even tracer for molecular hydrogen in the galaxy. OH does not rival CO in this matter, however, the data extracted from OH suggests that itself and other less common tracers are complimentary and can be used in conjunction with CO to paint a more complete picture of H_2. Using a mosaic of gas tracers to reveal the H_2 in the ISM can illuminate the CO-dark regions where H_2 is still present.

Cassiopeia A is a very small sample of the interstellar medium. As a result, the gas observed is not representative of the whole galaxy since the environmental conditions vary widely in the ISM Dawson et al. (2014). The way in which less abundant tracers compliment CO is on a very small scale, generally no more than a dozen arc-seconds based on the pixel resolution of Figure 8. Therefore, expanding this research would require observations at small scales against other bright radio sources rather than larger surveys of dense regions.

5. ACKNOWLEDGMENTS

R.P. and P.S. acknowledge the National Radio Astronomy Observatory (NRAO), Greenbank Observatory (GBO), the National Science Foundation (NSF), as well as Associated Universities Incorporated (AUI) for the capabilities to conduct this research. In addition, R.P and P.S. thank Dr. Ping Zhou at Nanjing University for the carbon monoxide data utilized in this analysis.

Facilities: Institute for Radio Astronomy in the Millimeter Range (IRAM, Sierra Nevada, Spain); The Expanded Very Large Array (EVLA, Socorro, New Mexico).

REFERENCES

Arias et al., M. 2018, Å, 612, 16, doi: 10.1051/0004-6361/201732411

Dawson, J., Walsh, A., Jones, P., et al. 2014, MNRAS, 439, 19, doi: 10.1093/mnras/stu032

Ebisawa, Y., Inokuma, H., Sakai, N., et al. 2015, ApJ, 815, 9, doi: 10.1088/0004-637X/815/1/13

Keohane, J. W., Rudnick, L., & Anderson, M. P. 1996, ApJ, 466, 7, doi: 10.1086/177511

Oonk, J. B. R., van Weeran, R. J., Salas, P., et al. 2017, MNRAS, 465, 23, doi: 10.1093/mnras/stw2818

Price-Whelan, A. M., Sipocz, B. M., & Gunther, H. M. 2018, , 156, 19, doi: 10.3847/1538-3881/aabc4f

Robitaille, T. P., Tollerud, E. J., & Greenfield, P. 2013, Å, 558, 9, doi: 10.1051/0004-6361/201322068

Salas, P., Oonk, J. B. R., van Weeran, R. J., et al. 2018, MNRAS, 475, 23, doi: 10.1093/mnras/stx3340

Weil, K. A., Fesen, R. A., Patnaude, D. J., et al. 2020, ApJ, 891, 15, doi: 10.3847/1538-4357/ab76bf

Zhou, P., Li, J.-T., Zhang, Z.-Y., et al. 2018, ApJ, 856, 13, doi: 10.3847/1538-4357/aad960